Mendeleev Commun., 2027, **37**, JUST ACCEPTED

Received 28.08.26
Revised 13.10.26

26/8184

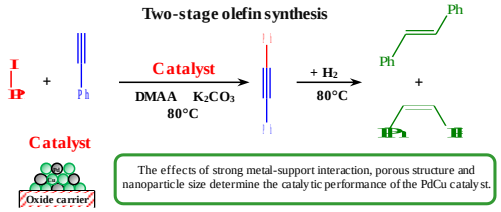
The influence of the support on the efficiency of Pd_1Cu_3 catalyst in two-step olefin synthesis

Alexander V. Rassolov,*[a] Alexandra S. Vishnevich,[a] Galina N. Baeva,[a] Dmitry P. Melnikov,[b] Ekaterina D. Patil[a] and Alexander Yu. Stakheev[a]

[a] *N. D. Zelinsky Institute of Organic Chemistry, Russian Academy of Sciences, 119991 Moscow, Russian Federation. E-mail: rav@ioc.ac.ru*
[b] *National University of Oil and Gas 'Gubkin University', 119991 Moscow, Russian Federation*

DOI: 10.71267/mencom.8184

Using CeO_2, TiO_2, Al_2O_3, and SiO_2 as examples, a comprehensive study was conducted to examine the influence of the nature of oxide supports on the efficiency of PdCu nanoparticles in the selective tandem synthesis of *cis*- and *trans*-stilbenes. The data obtained showed that the developed porous structure, nanoparticle size, and the effects of strong metal-support interactions are crucial at each stage of the process.



Keywords: oxide supports, tandem synthesis, bimetallic alloy, nanoparticle, Sonogashira cross-coupling, hydrogenation.

The development of new and improvement of existing catalytic compositions based on bimetallic alloy nanoparticles is a key area of modern research in synthetic and fine organic chemistry.[1] Its relevance is primarily driven by the need to create efficient, cost-effective, and environmentally friendly approaches to the targeted production of a wide range of valuable chemical products.[2]

In this context, a promising development in this area is the use of the tandem catalysis concept, which involves sequentially conducting several catalytic reactions in a single volume using a single catalyst.[3] This approach not only significantly reduces energy consumption, reagent use, and waste generation, but also facilitates the rapid production of target products in high yields. According to the literature, wide ranges of such tandem processes utilize cross-coupling reactions as one of their steps, during which a new carbon-carbon bond is formed.[4-7] The most prominent example of such reactions is the Sonogashira cross-coupling, traditionally carried out in the presence of homogeneous catalysts based on Pd and Cu (I) salts.[8,9]

In recent years, there has been a significant increase of interest in alternative methods for conducting both the Sonogashira reaction and multi-stage processes involving it in the presence of bimetallic catalysts based on PdCu nanoparticles.[10-14] This interest is driven by the excellent catalytic properties of alloyed nanoparticles, primarily due to the pronounced synergistic effects between Pd and Cu.[15] Their high thermal stability,[16] as well as the regenerate and reuse abilities, are also undeniable advantages.[17] The overwhelming majority of the presented research works come down to the fact that the Pd:Cu ratio[18] or careful optimization of each stage tandem process conditions plays a key role in the high efficiency of alloy nanoparticles.[7]

However, it should be noted that, in addition to these factors, the nature of the support used also significantly influences the stabilization and localization of active sites, as well as their structure and, consequently, the catalytic performance of PdCu nanoparticles. Traditionally, various highly porous functionally substituted polymers[19] and ordered mesoporous silicates[20,21] are used as supports in such processes, due to the specific features of the porous structure of these compositions, which ensure efficient mass transfer. However, the literature provides very few examples of tandem processes combining the Sonogashira reaction as one of the steps and the use of alloyed PdCu nanoparticles deposited on the surface of traditional oxide supports.[11,22,23]

The aim of this work was to conduct a comprehensive comparative study of bimetallic PdCu alloy catalysts deposited on the surface of various oxide supports for the tandem synthesis of olefins. This process involves the sequential Sonogashira reaction between iodobenzene and phenylacetylene and partial hydrogenation of the resulting product directly to *cis*- and *trans*-stilbenes. Commercially available oxides (CeO_2, TiO_2, Al_2O_3 an SiO_2) were used as supports in this study; a detailed description of their textural characteristics is presented in SI. The selection of specific support modifications is dictated not only by their thermal stability but also by the feasibility of determining the crystalline structure of the alloy nanoparticles via XRD, achieved by minimizing the overlap between support signals and the reflections characteristic of PdCu nanoparticles. The Cu and Pd contents in all samples were 5.4 and 3.0 wt %, respectively. For convenience, an atomic ratio of Pd:Cu = 1:3 is used in the further description of the results.

The diffraction patterns of individual supports (curves 2, 4, 6, 8) and bimetallic catalysts (curves 1, 3, 5, 7) are shown in Fig. 1a. Analysis of the obtained data allows us to conclude that in the case of Pd_1Cu_3/SiO_2, Pd_1Cu_3/TiO_2 and Pd_1Cu_3/Al_2O_3 (curves 3, 5 and 7), in addition to the reflections of the corresponding supports, signals were identified in the 2Θ angle range from 41.1° to 43.0° and from 48.4° to 50.0°. Comparison of the unit cell parameters with the ICDD crystallographic database, as well as quantitative calculations

© Mendeleev Communications.

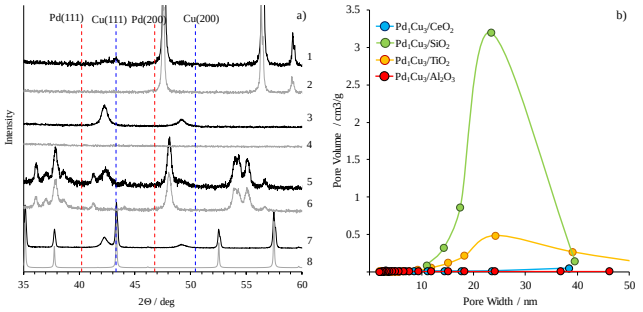


Figure 1 (a) XRD patterns of (1) Pd_1Cu_3/CeO_2, (3) Pd_1Cu_3/SiO_2, (5) Pd_1Cu_3/TiO_2, (7) Pd_1Cu_3/Al_2O_3, individual supports (2) CeO_2, (4) SiO_2, (6) TiO_2, (8) Al_2O_3 and (b) pore size distribution curves for bimetallic catalysts.

in the RIETAN-FP program, allow us to conclude that the indicated reflexes are related to reflections from the (111) and (200) planes of the Cu3Pd phase with a face-centered cubic lattice.[24] In the case of Pd_1Cu_3/CeO_2 (curve 1), the diffraction pattern is characterized by a set of signals related to the cubic lattice of CeO_2 (ICCD No. 43–1002), as well as a broad reflection with a maximum at 42.7° and a low-intensity shoulder at 49.7°, which can be attributed to reflections from the planes of the Cu3Pd phases. The maximum at 43.3° corresponds to the reflection from the (111) plane of metallic Cu. (ICDD No. 01–085–1326). It is noteworthy that, despite the identical ratio of components in each of the studied samples, the intensity of the alloy nanoparticles reflexes in the case of Pd_1Cu_3/TiO_2 and Pd_1Cu_3/CeO_2 is significantly lower than for other catalysts of the series. According to literature data, both CeO_2 and TiO_2 are prone to partial reduction under high-temperature reducing treatments, which in turn significantly induces metal-support interactions.[22,25,26] This suggests that such a significant difference in intensity may be due to the encapsulation of a certain proportion of bimetallic nanoparticles in the near surface supports layers.

The results of the study of the catalysts textural characteristics by the low-temperature nitrogen adsorption method (Fig. 1b, S3 and Table S1) allow us to conclude that, according to the IUPAC classification, the bimetallic samples belong to type IV mesoporous materials. The shape of the hysteresis loop according to the de Boer classification corresponds to type H1, which indicates the predominance of cylindrical pores. For the Pd_1Cu_3/SiO_2 and Pd_1Cu_3/TiO_2 samples, it was noted that the values of the average pore size (39.4 and 22.6 nm, respectively) and pore volume (0.87 and 0.21 cm^3/g) significantly exceed these indicators for other samples in the series. In the case of Pd/TiO_2, a more significant reduction in pore volume and average pore size is observed compared to the support. This may be attributed to pore blocking by relatively small metal nanoparticles, as well as local distortions in the near-surface TiO_2 layers resulting from strong interaction effects.[25] At the same time, the obtained data allow us to conclude that the application of the active phase to the SiO_2 and TiO_2 surface has virtually no effect on the change in the average pore size, which can positively affect the mass transfer and the desorption rate of the formed products at each stage of the two-stage synthesis.

During the study of the surface structure of the samples by IR-spectroscopy of adsorbed CO (Fig. S1), it was established that the spectrum of the Pd/TiO_2 reference sample is characterized by absorption bands (AB) with maxima at 2084 cm^{-1}, 1979 cm^{-1} and 1934 cm^{-1}. Their positions correspond to the stretching vibrations of CO molecules coordinated with one (linear adsorption), two adjacent (bridged adsorption) and three Pd atoms (multicoordinated adsorption), respectively.[27,28] In the spectrum of Cu/TiO_2, a broad intense AB with maxima at 2120 cm^{-1} and 2111 cm^{-1} was identified, related to the vibrations of CO molecules adsorbed on Cu^{2+} and Cu^+ sites, respectively.[29] Analysis of the spectra of bimetallic catalysts showed that all samples are characterized by the formation of Pd_1 adsorption sites, as evidenced by the AB, the maxima of which are located in the range from 2087 cm^{-1} in the case of Pd_1Cu_3/TiO_2 to 2066 cm^{-1} in the case of Pd_1Cu_3/Al_2O_3.

However, despite their qualitatively similar character, the spectra of Pd_1Cu_3/TiO_2 and Pd_1Cu_3/CeO_2 are distinguished by the presence of asymmetrical bands related to CO complexes with Cu^+ ions (maxima at 2119 – 2116 cm^{-1}), the intensity of which significantly exceeds the linearly adsorbed CO band. This may indicate partial screening of surface Pd by Cu atoms. For Pd_1Cu_3/Al_2O_3 and Pd_1Cu_3/SiO_2 samples, a shift of the linearly adsorbed CO band maximum (2066 and 2078 cm^{-1}, respectively) toward lower wavenumbers is observed relative to the position for monometallic Pd (2084 cm^{-1}). This shift is attributed to an increase in electron density on the Pd resulting from electron density redistribution among the alloy atoms. In turn, this may facilitate increased electron density donation into the antibonding orbitals of the CO molecule and a reduction in the C–O stretching frequency.[30]

The nature of the support also has a significant impact on the morphology and size distribution of the nanoparticles (Fig. S2). For example, in the case of Pd_1Cu_3/CeO_2, irregularly shaped nanoparticles are formed, randomly distributed over the support surface. The nanoparticle size distribution range is quite wide (from 4 to 40 nm), and the histogram is characterized by the presence of several maxima at 8 and 24 nm, indicating a bimodal distribution. For the Pd_1Cu_3/SiO_2 catalyst, a wide size range (from 6 to 46 nm) is also observed, with a maximum at 21.2 nm. The nanoparticles are predominantly near-spherical in shape but are distributed unevenly across the support. In the case of Pd_1Cu_3/Al_2O_3 and Pd_1Cu_3/TiO_2, the distribution from 2 to 24 nm is monomodal, and the nanoparticles have a spherical shape with an average size of 8.2 and 16.4 nm, respectively. Moreover, the proportion of relatively small nanoparticles with an average size of 6 to 8 nm ranges from 21% to 18%.

The main results of the study of the catalytic characteristics at the first stage of the tandem process (cross-coupling) are shown in Fig. 2a, b. It can be concluded that the catalytic activity increases in the series of bimetallic catalysts depending on the support in the following order: $CeO_2<Al_2O_3<SiO_2<<TiO_2$. The minimum values of phenylacetylene conversion (X_{PhA}^{8h}) are characteristic of Pd_1Cu_3/CeO_2 and Pd_1Cu_3/Al_2O_3 (X_{PhA}^{8h} = 26.0% and 32.3%, respectively). It is noteworthy that in the case of Pd_1Cu_3/SiO_2, an almost linear increase in X_{PhA} is observed with the reaction progress from 13% at 2 h to 48% at 8 h. Moreover, the minimum selectivity for diphenylacetylene (DPhA) is 88.8%, which exceeds the indicators of other Pd_1Cu_3 catalysts studied in the work. In addition to the target product of the first stage (DPhA), gas chromatography-mass spectrometry revealed the formation of another carbon-containing product, namely, 1,4-diphenylbutadiene, which is associated with a parallel Glaser-Hey homocoupling side reaction of the starting phenylacetylene at active Cu sites.[31] The first stage of the process is most active in the presence of the Pd_1Cu_3/TiO_2 catalyst. In this case, the conversion of PhA after just 2 h of reaction is 45.4%, while X_{PhA}^{8h} = 89.4%. The selectivity for DPhA is practically constant, regardless of the reaction time, and varies from 77.0% to 81.3%. The obtained result is in good agreement with the data presented in the work.[22] The authors report that depositing metallic nanoparticles on the surface of reducible oxides (such as TiO_2 and CeO_2) with a sufficiently developed porous structure promotes a more active and selective cross-coupling reaction of phenylacetylene and iodobenzene, compared to the results obtained using non-reducible oxides such as Al_2O_3 and SiO_2. Furthermore, the authors claim that this effect is most pronounced for relatively

© Mendeleev Communications.

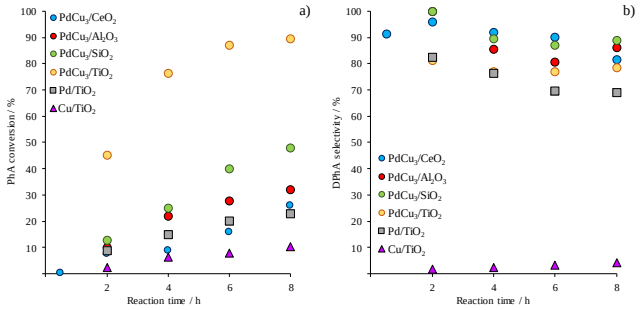


Figure 2 PhA conversion (a) and DPhA selectivity (b) dependences on the reaction time at the cross-coupling of iodobenzene and phenylacetylene for monometallic Pd/TiO_2, Cu/TiO_2 and bimetallic Pd_1Cu_3 catalysts, supported on CeO_2, Al_2O_3, SiO_2 and TiO_2.

small nanoparticles with an average size of 4 to 14 nm. In this regard, it can be assumed that the less pronounced activity increase in the case of Pd_1Cu_3/CeO_2 relative to the Pd_1Cu_3/TiO_2 catalyst at the first stage of the process may be a consequence of a less developed porous structure. In addition, the activity and selectivity of bimetallic Pd_1Cu_3/TiO_2 significantly exceeds the performance of monometallic Cu/TiO_2 and Pd/TiO_2 samples, which also corresponds to the results we obtained earlier.[32,33]

A similar dependence of activity on reaction time is observed in the second stage of the tandem process (hydrogenation). In the presence of the monometallic Cu/TiO_2 catalyst, the conversion of DPhA does not exceed 0.1%, which is attributed to the extremely low catalytic activity of this sample in the hydrogenation reaction.[32] For bimetallic samples, the conversion of DPhA (formed during the first stage) after 16 h of reaction ranges from 4.3% (for Pd_1Cu_3/CeO_2) to 9.9% and 12.0% (for Pd_1Cu_3/Al_2O_3 and Pd_1Cu_3/SiO_2, respectively). Complete conversion of DPhA was achieved only in the presence of Pd/TiO_2 and Pd_1Cu_3/TiO_2 catalysts. The hydrogenation rate at the alkyne-to-olefin stage for Pd/TiO_2 is $r_1 = 7.01$ mmol/(min·g_{cat}), while the selectivity toward the target products is 90.9%. In the presence of Pd_1Cu_3/TiO_2, hydrogenation proceeds significantly more slowly ($r_1 = 0.053$ mmol/(min·g_{cat})). With bimetallic catalysts, the selectivity toward stilbenes is virtually independent of the support used and amounts to 97–98%.

Thus, the obtained experimental data, combined with the results of a comprehensive physicochemical study, allow us to conclude that the most promising results in two-stage olefin synthesis can be achieved using TiO_2 as a support. A comparison of the obtained experimental data with the results of a comprehensive physicochemical study of Pd_1Cu_3 catalysts suggests that the developed porous structure of the support, the average size of the bimetallic nanoparticles, and the effects of strong metal-support interactions have a key influence on the catalyst's efficiency during each stage of tandem olefin synthesis.

This work was supported by the Russian Science Foundation (grant no. 25-73-00079).

Low temperature nitrogen adsorption-desorption was performed in the Center for Advanced Catalytic Technologies of Zelinsky Institute of Organic Chemistry, Moscow.

Online Supplementary Materials

Supplementary data associated with this article can be found in the online version at doi: 10.71267/mencom.8184.___

References

1. B. Wang, Y. Wang, J. Li, X. Guo, G. Bai, X. Tong, G. Jin and X. Guo, *Catal. Sci. Technol.*, 2018, **8**, 3357-3362; https://doi.org/10.1039/c8cy00618k
2. B. M. Trost, *Acc. Chem. Res.*, 2002, **35**, 695-705; https://doi.org/10.1021/ar010068z
3. S. F. Mayer, W. Kroutil and K. Faber, *Chem. Soc. Rev.*, 2001, **30**, 332-339; https://doi.org/10.1039/b105493g
4. C. C. Wu, R. Ambre, M. H. Lee and J. J. Shie, *Org. Lett.*, 2022, **24**, 2889-2893; https://doi.org/10.1021/acs.orglett.2c00891
5. Y. N. Kotovshchikov, A. A. Binyakovsky, G. V. Latyshev, N. V. Lukashev and I. P. Beletskaya, *Org. Biomol. Chem.*, 2022, **20**, 7650-7657; https://doi.org/10.1039/d2ob01267g
6. P. Y. Choy, K. B. Gan and F. Y. Kwong, *Chin. J. Chem.*, 2023, **41**, 1099-1118; https://doi.org/10.1002/cjoc.202200703
7. D. Lasanyi, A. Meszaros, Z. Novak and G. L. Tolnai, *J. Org. Chem.*, 2018, **83**, 8281-8291; https://doi.org/10.1021/acs.joc.8b00998
8. M. Bakherad, *Appl. Organomet. Chem.*, 2013, **27**, 125-140; https://doi.org/10.1002/aoc.2931
9. F. Mohajer, M. M. Heravi, V. Zadsirjan and N. Poormohammad, *RSC Adv.*, 2021, **11**, 6885-6925; https://doi.org/10.1039/d0ra10575a
10. R. Yan, H. Yin, X. Zuo, W. Peng, X. Zhu, L. Shi, J. Hou, D. Wang, F. Ye, J. Li, B. Mao and C. Hu, *Appl. Catal. B: Environ.*, 2025, **361**, 124609; https://doi.org/10.1016/j.apcatb.2024.124609
11. J. Zhang, M. Huang, Y. Xu, J. Yin, X. Zhang and J. Zhang, *ACS Catal.*, 2025, **15**, 14348-14365; https://doi.org/10.1021/acscatal.5c03964
12. A. Reina, T. Dang-Bao, I. Guerrero-Rios and M. Gomez, *Nanomaterials (Basel)*, 2021, **11**; https://doi.org/10.3390/nano11081891
13. T. Dang-Bao, C. Pradel, I. Favier and M. Gómez, *ACS Appl. Nano Mater.*, 2019, **2**, 1033-1044; https://doi.org/10.1021/acsanm.8b02316
14. B. Wu, T. Lin, M. Huang, S. Li, J. Li, X. Yu, R. Yang, F. Sun, Z. Jiang, Y. Sun and L. Zhong, *Angew. Chem. Int. Ed. Engl.*, 2022, **61**, e202204116; https://doi.org/10.1002/anie.202204116
15. Z. Qiao, F. Wang, Y. Zhang, J. Guan, Z. Li, X. Wang, X. Liu and Y. Huang, *Angew. Chem. Int. Ed. Engl.*, 2026, **65**, e9988326; https://doi.org/10.1002/anie.9988326
16. Q. Liu, X. Wang, L. Li, K. Song, Y. Wang and P. Qian, *RSC Adv.*, 2021, **12**, 62-71; https://doi.org/10.1039/d1ra07581k
17. M. Annapurna, T. Parsharamulu, P. Vishnuvardhan Reddy, M. Suresh, P. R. Likhar and M. Lakshmi Kantam, *Appl. Organomet. Chem.*, 2015, **29**, 234-239; https://doi.org/10.1002/aoc.3277
18. A. Mastalir, *Molecules*, 2024, **29**; https://doi.org/10.3390/molecules29245857
19. M. N. A. Bakhvalova E.S., Bykov A.V., Nikoshvili L.Z., *Chem. Eng. Trans.*, 2024, **114**, 97-102; https://doi.org/10.3303/CET24114017
20. D. Chakraborty, A. Bhaumik, *Catalysts*, 2024, **15**, 16; https://doi.org/10.3390/catal15010016
21. C. Liu, B. Qiao and T. Zhang, *JACS Au*, 2024, **4**, 4129-4140; https://doi.org/10.1021/jacsau.4c00784
22. S. Sisodiya, L. R. Wallenberg, E. Lewin and O. F. Wendt, *Appl. Catal. A-Gen.*, 2015, **503**, 69-76; https://doi.org/10.1016/j.apcata.2015.07.001
23. Z. Li, H. Liu, A. Pang, S. Ji, X. Lu, Y. Zhang, C. Guo, L. Bai, J. H. Horton and Y. Wang, *Adv. Funct. Mater.*, 2025, **35**, e05655; https://doi.org/10.1002/adfm.202505655
24. A. V. Rassolov, G. N. Baeva, I. S. Mashkovsky and A. Y. Stakheev, *Mendeleev Commun.*, 2018, **28**, 538-540; https://doi.org/10.1016/j.mencom.2018.09.030
25. K. Vikrant, M. W. Chung, S. Weon, D. W. Boukhvalov, B. Baitimbetova, P. M. Heynderickx, K.-H. Kim and E. E. Kwon, *J. Sci.: Adv. Mater. Devices*, 2026, **11**, 101279; https://doi.org/10.1016/j.jsamd.2026.101279
26. N. Tsubaki and K. Fujimoto, *Top. Catal.*, 2003, **22**, 325-335; https://doi.org/10.1023/a:1023548608733
27. C. Lentz, S. P. Jand, J. Melke, C. Roth and P. Kaghazchi, *J. Mol. Catal. A: Chem.*, 2017, **426**, 1-9; https://doi.org/10.1016/j.molcata.2016.10.002
28. G. Agostini, R. Pellegrini, G. Leofanti, L. Bertinetti, S. Bertarione, E. Groppo, A. Zecchina and C. Lamberti, *J. Phys.*

© Mendeleev Communications.

Chem. C, 2009, **113**, 10485-10492; https://doi.org/10.1021/jp9023712
29. M. B. Padley, C. H. Rochester, G. J. Hutchings and F. King, *J. Catal.*, 1994, **148**, 438-452; https://doi.org/10.1006/jcat.1994.1230
30. P. V. Markov, G. O. Bragina, G. N. Baeva, O. P. Tkachenko, I. S. Mashkovsky, I. A. Yakushev, N. Y. Kozitsyna, M. N. Vargaftik and A. Y. Stakheev, *Kinet. Catal.*, 2015, **56**, 591-597; https://doi.org/10.1134/s0023158415050122
31. J. Aromaa, M. Kekkonen, M. Mousapour, A. Jokilaakso and M. Lundström, *Corros. mater. degrad.*, 2021, **2**, 625-640; https://doi.org/10.3390/cmd2040033
32. A.V Rassolov., A.S.Vishnevich, E.D.Patil, G.N.Baeva, A.Yu.Stacheev, *Kinet. Catal*., 2026, **67**, 103-107; https://doi.org/10.7868/S3034541326010088
33. A. V. Rassolov, A. S. Vishnevich, E. D. Patil, G. N. Baeva, D. P. Melnikov, D. A. Bokarev, A. Yu. Stakheev, *Mendeleev Commun.*, 2026, **36**, 576-578; https://doi.org/10.71267/mencom.8060

Received: 28th August 2026; Com. 26/8184

© Mendeleev Communications.